electronics

Article

Using the Variable Geometry in a Planar Inductor for an Optimised Performance

Maha Aldoumani *, Baris Yuce and Dibin Zhu

College of Engineering, Mathematics, and Physical Sciences, University of Exeter, Harrison Building, North Park Road, Exeter EX4 4QF, UK; B.Yuce@exeter.ac.uk (B.Y.); D.Zhu@exeter.ac.uk (D.Z.)
* Correspondence: ma793@exeter.ac.uk

Abstract: In this paper, the performance, modelling and application of a planar electromagnetic sensor are discussed. Due to the small size profiles and their non-contact nature, planar sensors are widely used due to their simple and basic design. The paper discusses the experimentation and the finite element modelling (FEM) performed for developing the design of planar coils. In addition, the paper investigates the performance of various topologies of planar sensors when they are used in inductive sensing. This technique has been applied to develop a new displacement sensor. The ANSYS Maxwell FEM package has been used to analyse the models while varying the topologies of the coils. For this purpose, different models in FEM were constructed and then tested with topologies such as circular, square and hexagon coil configurations. The described methodology is considered an effective way for the development of sensors based on planar coils with better performance. Moreover, it also confirms a good correlation between the experimental data and the FEM models. Once the best topology is chosen based on performance, an optimisation exercise was then carried out using uncertainty models. That is, the influence of variables such as number of turns and the spacing between the coils on the output inductance has been investigated. This means that the combined effects of these two variables on the output inductance was studied to obtain the optimum values for the number of turns and the spacing between the coils that provided the highest level of inductance from the coils. Integrated sensor systems are a pre-requisite for developing the concept of smart cities in practice due to the fact that the individual sensors can hardly meet the demands of smart cities for complex information. This paper provides an overview of the theoretical concept of smart cities and the integrated sensor systems.

Keywords: electromagnetic sensors; ANSYS Maxwell FEM modelling; planar electromagnetic coils; uncertainty; optimisation; robust design

check for updates

Citation: Aldoumani, M.; Yuce, B.; Zhu, D. Using the Variable Geometry in a Planar Inductor for an Optimised Performance. *Electronics* **2021**, *10*, 721. https://doi.org/10.3390/electronics10060721

Academic Editor: Massimo Donelli

Received: 2 February 2021
Accepted: 13 March 2021
Published: 18 March 2021

Publisher's Note: MDPI stays neutral with regard to jurisdictional claims in published maps and institutional affiliations.

Copyright: © 2021 by the authors. Licensee MDPI, Basel, Switzerland. This article is an open access article distributed under the terms and conditions of the Creative Commons Attribution (CC BY) license (https://creativecommons.org/licenses/by/4.0/).

1. Introduction

1.1. Applications of Sending Techniques

Smart cities have started to be emerging environments across the globe in which these systems have become data production centres from urban environments, buildings, vehicles, traffics, public offices, water systems [1]. Such a huge number of data helps scientists, policy and rule makers and other stakeholders to generate the most appropriate decisions. Hence, the sensory-based infrastructure has become the key concept for GPS, RFID scanners, magnetometers, Light Detection and Ranging (LIDARs), temperature and humidity air pressure measurements. Furthermore, such a concept finds applications in smart parking, structural health, smartphone detection, electromagnetic field levels, traffic congestion and smart lighting. The most widely used application of such a concept is the electromagnetic sensing system [2,3]. Sensors are important and substantial for any intelligent control system. A process is improved based on its environment and this requires a control system typically equipped with an array of sensors from which it collects the required data. One of the important applications of integrated sensor system is the Smart Transport and Mobility Tracking system since this is needed to avoid and optimise the traffic flows on roads. As smart cities prevail with a rising ability to be instrumented, various movable and fixed sensors, connected through wired and wireless network, are implemented. Such applications include adaptive and personalised maps, vehicle navigation, traffic monitoring and road incident detection [1–4]. A few years back, researchers have been made aware of the planar type of electromagnetic sensors and the possible defects in printed circuit boards (PCBs). The study of such planar type systems for sensing has been extended to evaluate properties related to the near surface material such as permeability, conductivity and permittivity.

The non-invasive techniques used for determining the properties of a component or structure, coherence of a material or the quantitative measure of characteristics of any object is termed as non-destructive testing (also known as NDT). Such methods can be easily used, without harming or damaging the system, for inspection and measurement. Recently, the NDT has been found in various applications and industries. The demand for the utilisation of appropriate techniques is increasing with the increase in demand of a greater performance techniques for inspection. For operation in severe environments, the use of NDT approaches is considered a necessity [1–4]. Nowadays, due to the application of sensing principles in the non-destructive evaluation (NDE) and the wireless power transmission [4], the power coil technology has been renewed. The advantages of planar coils are more than those provided by the traditionally wound coils due to the former's wireless sensing capabilities when compared to the latter [5], small size profiles [6,7], higher levels of robustness [8,9] and the lower cost. Based on the application [10–12], these planar coils can be manufactured on hard or flexible substrates [13,14]. The inductance of a planar coil is affected by both the electromagnetic [15,16] and the physical factors and these are frequently implemented as a part of an inductance-capacitor (LC) circuit [17]. Any change in the value of the inductance affects the resonance of the circuit [18–20]. Such characteristics allow for various effective applications which include NDT and NDE [21–23], health monitoring [24,25], sensing techniques and wireless power transfer [26,27]. To monitor and capture the various physical aspects of the external environment, e.g., light, temperature, humidity, magnetic fields and sound, there exists a handful of sensor types capable of fulfilling such purposes [28]. Integrated sensor systems involve the use of multiple complementary sensors within Micro-Electro-Mechanical Systems (MEMS) [29]. Apart from the internal connections of sensors, in the context of smart cities, it is important for them to be externally connected via wireless networks to a central unit that receives and processes the data, hence called wireless sensor networks [30,31]. That is important because cities are too complex for a single type of sensor to satisfy the demands for the analysis of information necessary for the smart management.

1.2. The Scope of the Paper

In this paper, the planar coils, being a part of a displacement sensor, will be investigated and an overview of the typical sensor types and their corresponding urban applications are discussed. This research presents a key development of the electromagnetic sensors by analysing the behaviour of different planar coils for tracking and location identification for the smart cities. The ANSYS Maxwell 3D FEM software package has been used for the evaluation of the different coil topologies: circular, square and hexagon coils. Then, an impedance analyser was used for characterising the manufactured versions. A comparison of both the measured and simulated performance of each design sensor is presented in this paper.

In order to study the interaction of magnetic, dielectric and conducting materials, sensors of a planar type such as circular, square and hexagon configurations were designed and fabricated. These sensors have a simple structure and are planar in nature. A simple fabrication technology, i.e., printed circuit boards (PCBs), is used for fabricating such sensors. The principle for operating these sensors is dependent on the interaction of the electromagnetic field, which is produced by the sensor, and the neighbouring materials to be tested. There are two coils in these sensors, namely: the sensing coil and the exciting coil. Alternating current is carried by the exciting coil which generates an electromagnetic field of a high frequency that penetrates in the system under investigation. In the process, eddy currents are generated on the system by the electromagnetic field induced by the system under investigation. The materials which are used for investigation is of magnetic and conducting properties. The generated field in the system is modified by the field induced due to the flow of the eddy current. The resultant field is diagnosed by the coil which is placed above the exciting coil. The coil which detects the field is the sensing coil or 'pick up' coil. Amongst the utilised coil geometries, the hexagon type sensor when used for detecting cracks in metals, for instance, has a poor performance as it is affected by the non-homogeneity of the material as well as the alignment of the cracks. Hence, the square type sensors were developed to overcome such issues [3]. Furthermore, the circular pattern is less influenced by the developed eddy currents and this results in less dependence on the geometry or alignment of the sensors when compared to the other configurations.

2. Methodology

2.1. The Experimental Method

The following design parameters, Table 1, are typically related to the board level inductor design utilised in the experiment. The coils used for experimental measurements have the same dimensions with the ones used for simulation purposes.

Table 1. The structural parameters of the proposed Printed Circuit Board (PCB) inductor.

Parameter	Unit	Value
Inner radius (R)	mm	0.15
Width of the copper track (W)	mm	0.1
Gap between the copper tracks	mm	0.2
Thickness of the copper (Th)	mil	2.5
Distance between two layers (D)	mm	0.5
Turns in a single layer (N)		12

In terms of coils, they are all constructed of copper. Several calibration holes are set on the board for a precise angular adjustment. By using a commercial 2-layer PCB fabrication process, different sets of inductors were fabricated. The setup of the fabricated coils is shown in Figure 1. A 2-port Agilent network analyser has been used to measure the excitation of the fabricated inductors. The short-open-load-through (SOLT) calibration method has been used to calibrate the network analyser by standard calibration tools. The S-parameters (S_{11}, S_{12}, S_{21}, and S_{22}) were measured for each inductor using the network analyser. The values of the inductance for each design were obtained from the Y-parameter data.

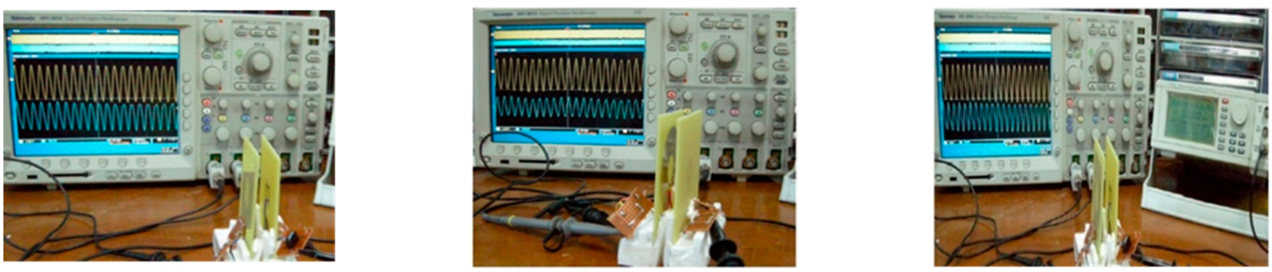

(**a**) (**b**) (**c**)

Figure 1. The fabricated coils on the PCB, for 3D printed support structures: (**a**) square coil topology; (**b**) circular coil topology; (**c**) hexagon topology.

2.2. The Analytical Method

A leakage inductance might develop through the transmission of electrical energy between the primary and the secondary coil. In the intervening period of time, a mutual inductance is produced due to the magnetic flux from the primary coil that cuts through the secondary coil to induce the voltage and the current in the secondary coil. Occasionally, the mutual inductance can be lower than that of the leakage inductance, which leads to minimising the magnetising flux. The relationship that is used to calculate the mutual inductance is given by Equation (1) [3]:

$$M = \sqrt{L_1\, L_2} \tag{1}$$

where L_1 is the inductance of the primary coil and L_2 is the inductance of the secondary coil. The power transferred to the sensing coil, P, can be calculated by Equation (2) [3]:

$$P = f \cdot M^2 \cdot I_p^2 / L_2 \tag{2}$$

where f is the frequency and I_p is the current in the primary coil. From this relationship, it is known that the output power (P) is restricted by the mutual inductance. In this context, the mutual inductance can be calculated using many different formulae such as the Neumann's Integrals method and the Maxwell formulae as well as the use of finite element analysis (FEA). When the FEA approach is applied, the Ansys software can be utilised to simulate the output of the coils and this can provide an accurate performance using built-in advanced calculation techniques. An illustration of the stages in FEA modelling is shown in Figure 2.

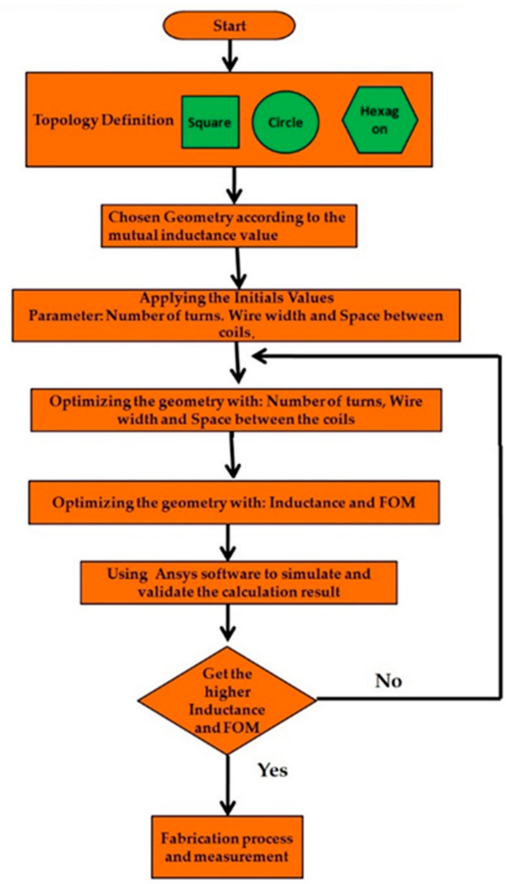

Figure 2. The stages involved in Finite Element Analysis (FEA) modelling of the proposed design.

2.3. The Modelling Method

The Maxwell 3d of Ansys Electronics desktop 18 Suite was utilised to simulate the different types of coils. This simulation investigates the mutual inductance or the coupling coefficient between two identical coils of which one acts as the transmitter while the other acts as the receiver. The magnetic fields generated by a defined DC current in the transmitter coil and the correspondence with the receiver coil, i.e., TX and RX, respectively, are thoroughly studied. The Ansys Maxwell software has been used to compare various coil shapes (circular, square, and hexagonal). The generated coils using Ansys Maxwell are shown in Figure 3. The features of each coil design with regards to the number of turns, thickness and space between the traces are shown in Table 2. In this context, the space between the traces was varied according to the desired pitch value.

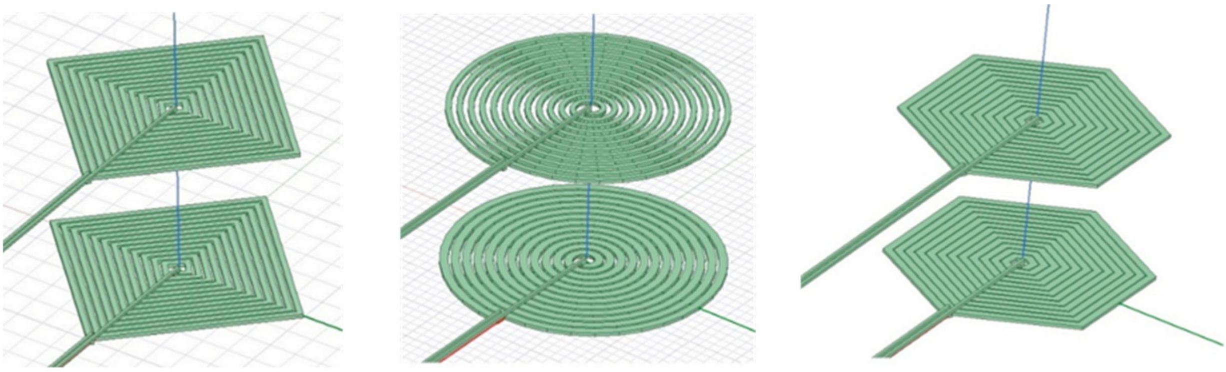

Figure 3. The various topologies of the modelled coils: square, circular and hexagonal, respectively.

Table 2. The various features of the designed coils.

Coil ID	Coil Geometry	Number of Turns	Thickness (mil)	The Space between the Excitation and Sensing Coils (mm)		
				Option 1	Option 2	Option3
Circular		12	2.5	0.5	1	1.5
Square		12	2.5	0.5	1	1.5
Hexagonal		12	2.5	0.5	1	1.5

2.4. The Robust Design Method

The Meta-model-based design optimisation is becoming increasingly popular in the industrial practice for the optimisation of complex engineering problems, especially to reduce the burden of computationally expensive simulations [32]. The idea behind the Meta-model-based design optimisation is to build a surrogate model (or a meta-model) from a reduced number of simulations runs and subsequently use the model for optimisation purposes [32–34]. The surrogate model, i.e., $y = f\ (x_1, x_2 \ldots,\ x_n)$, approximates the relationship between the design variables, i.e., $x_1, x_2 \ldots,\ x_n$, and the output variable, y [32,33]. This method can speed up the design optimisation process since the function evaluations of the surrogate model are less expensive to execute when compared to deterministic simulations. The simplest type of 'Response Surface' is a linear model in which the functional relationship $f\ (x_1, x_2 \ldots,\ x_n)$ is assumed to be a linear function of the design variables [34]. Linear models can be extended to polynomial response surface models wherein the response surface is a polynomial function of the design variables. In either way, the linear or higher order response surface (polynomials) can be obtained using the 'Ordinary Least Squared' approach by minimising the sum of the squared distances of a given data points from the surface [35]. In this case, the surrogate modelling utilising the least squared approach assumes that all errors are normally distributed with given mean and variance [32]. This assumption is often too stringent in real-world problems [32–35].

The Kriging method has been pre-fixed with different names depending on the form of the regression function, $f\ (x)$. For instance, the simple Kriging method assumes that $f\ (x)$ is a known constant, i.e., $f\ (x) = 0$. On the other hand, the ordinary Kriging approach assumes that $f\ (x)$ is constant but unknown, i.e., $f\ (x) = a_0$. For more complex processes, trend functions might be linear or quadratic polynomials. In this regard, the universal Kriging treats the trend function as a multi-variate polynomial such that [32]:

$$f(x) = \sum_{i=1}^{p} \alpha_i b_i(x) \tag{3}$$

where $b_i(x) = b_1(x),\ b_2(x) \cdots,\ b_p(x)$, are the basis functions (e.g., the power base for a polynomial) and $\alpha_i = (\alpha_1,\ \alpha_2 \cdots, \alpha_p)$ denote the coefficients. The idea is that the regression function captures the largest variance in the data (the general trend) and then the Gaussian Process interpolates the residuals [27–32]. In fact, the regression function $f(x)$ is the mean of the broader Gaussian Process Y.

One of the most widely used Kriging approaches is the Blind Kriging method. In this approach, the trend function $f(x)$ is unknown and is hard to choose for a given problem [32–34]. Some feature selection methods sometimes offer the possibility to identify the most plausible interactions occurring in the data [32]. The Blind Kriging is used to efficiently determine the base functions, or features, that capture the most variance in the sample data [33]. In this respect, a set of candidate functions is considered from which to choose for the problem. In the ideal case the sample data are almost fully represented by the chosen trend function and the stochastic process $Z(x)$ has little or no influence [32]. The idea is to select new features to be incorporated in the regression function of this Kriging model, considering features that are already a part of the regression function of the model. The whole set of candidate functions that is used to fit the data in a linear model are given by Equation (4) [32]:

$$g(x) = \sum_{i=1}^{p} \alpha_i b_i(x) + \sum_{i=1}^{t} \beta_i c_i(x) \tag{4}$$

where t is the number of candidate functions. The first part of this equation is the regression function of Kriging and, hence, the coefficients of α have already been determined independently of $\beta = (\beta_1, \cdots, \beta_t)$. The estimation of β provides a relevance score of the candidate features [33,34]. A frequentist estimation of β (e.g., the least-squares solution) would be a straightforward approach to rank the features (e.g., the least-squares solution) [32–35].

3. Results and Discussion

3.1. The Experimental Results

The spacing distance between the coils changes the effective inductance value as shown in Figure 4. It is evident that the increase in the spacing distance causes a gradual decrease in the value of the generated inductance. The results were obtained from measurements of actual displacement. It can be seen that for any given spacing value, the squared coil configuration has provided the highest level of inductance compared to the hexagonal and circular designs. Furthermore, it can be seen that the larger the spacing the lower the generated inductance and this applies to all design configurations. As the spacing value increases, the generated inductance obtained from all designs converges and this means that at larger spacing values, it becomes less dependent on the coil configuration.

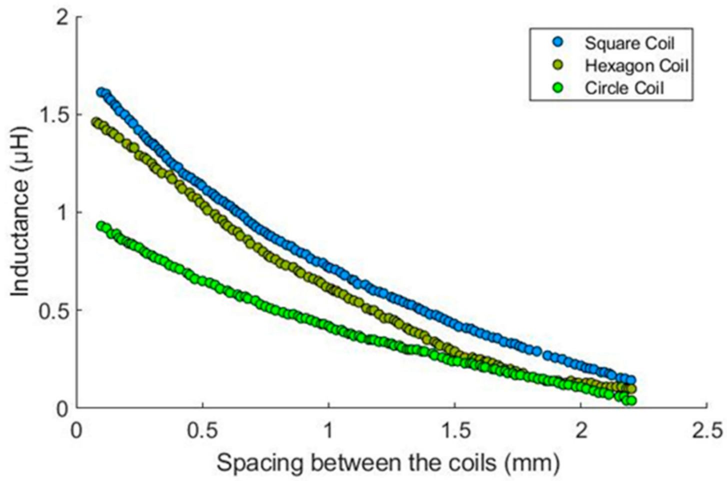

Figure 4. The experimental result between the resulting inductance and the spacing between the excitation and sensing coils.

3.2. The Modelling and Optimisation Results

To compare the effectiveness of the three proposed coil designs, the Ansys Maxwell electromagnetic software has been employed to analyse the distribution of the magnetic flux density in the magnetic cores o the excited sensors. To simplify the design diversity despite the distinct geometric designs of the excitation coils, key design factors were maintained unchanged through the various designs to allow for comparisons. This includes the number of wires turns, the metal wire gap, the cross-sectional area of the metal wire, the coil resistance, the coil inductance and the dimensions of the ferromagnetic core. Therefore, by assuming a uniform excitation currents through the coils, the simulation results, Figure 5, provide an approximate solution of the electromagnetic excitation condition via the excitation coils and the magnetisation of the magnetic cores. From the obtained results in Figure 5, it can be seen that the highest flux density recorded for the square coils was 5.55×10^{-4} T with a lowest value of 2.59×10^{-5} T. It is also evident that for this particular design, the highest flux is recorded at the centre of the coil which decreases towards the circumference of the coil, i.e., in the radial direction. On the other hand, the hexagonal coil design provided a lower maximum flux value when compared to the square coil design. The maximum value for the hexagonal design was around 4.006×10^{-4} T at the centre of the coil which, again, decreased towards the circumference of the coil, i.e., in the radial direction. The lowest value for this specific coil design was around 3.77×10^{-5} T. The flux values were lowest for the circular design with a maximum of 3.99×10^{-4} T at the centre and 6.49×10^{-5} T nearby the circumference.

Overall, the square coil design provided the highest possible flux density followed by the hexagonal and then the circular geometry. This was also the case while changing the spacing distance between the coils, Figure 6. It can be seen that for any given spacing value, the squared coil configuration has provided the highest level of inductance compared to the hexagonal and circular designs. Furthermore, it can be seen that the larger the spacing the lower the generated inductance and this applies to all design configurations. As the spacing value increases, the generated inductance obtained from all designs converges and this means that at larger spacing values, it becomes less dependent on the coil configuration.

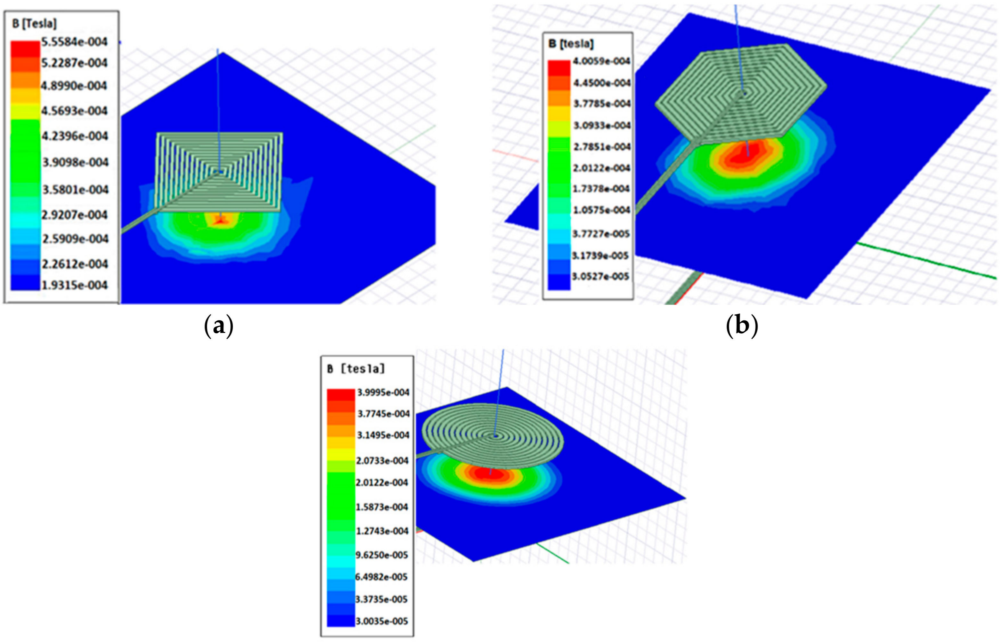

Figure 5. The modelling and simulation results of the square (a), hexagonal (b) and circular (c) coil topologies.

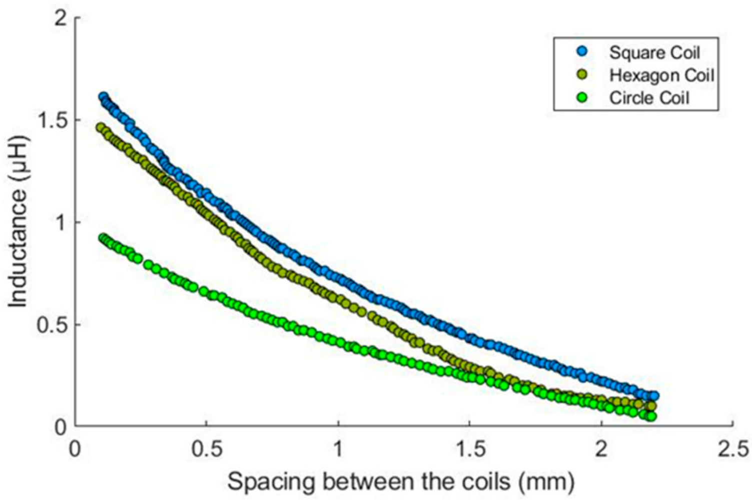

Figure 6. The simulation results of varying the spacing distance between excitation and the sensing coils.

The purpose of the proposed design in the current paper is to optimise the design of the PCB inductor for tracking and location identification in the applications of smart cities. As such, it is desirable to achieve the highest possible inductance. The Figure-Of-Merit (FOM) of an inductor is given by equation [31]:

$$\mathrm{FOM} = \frac{L}{A} \tag{5}$$

where L is the inductance (μH) and A is the area of the coil (mm^2). The target of optimisation is to obtain the maximum possible FOM values from the given design configurations. The results in Figure 7 show the effects of changing the number of turns and the spacing between the coils on the value of the FOM for the square, hexagonal and circular configurations, respectively. The general trend in these figures is that the higher the number of turns, the larger the value of the FOM and hence the output inductance. On the contrary, the larger the spacing between the coils the lower the value of the FOM. Amongst all, the square coil design provides the highest FOM at any given number of turns or a spacing value.

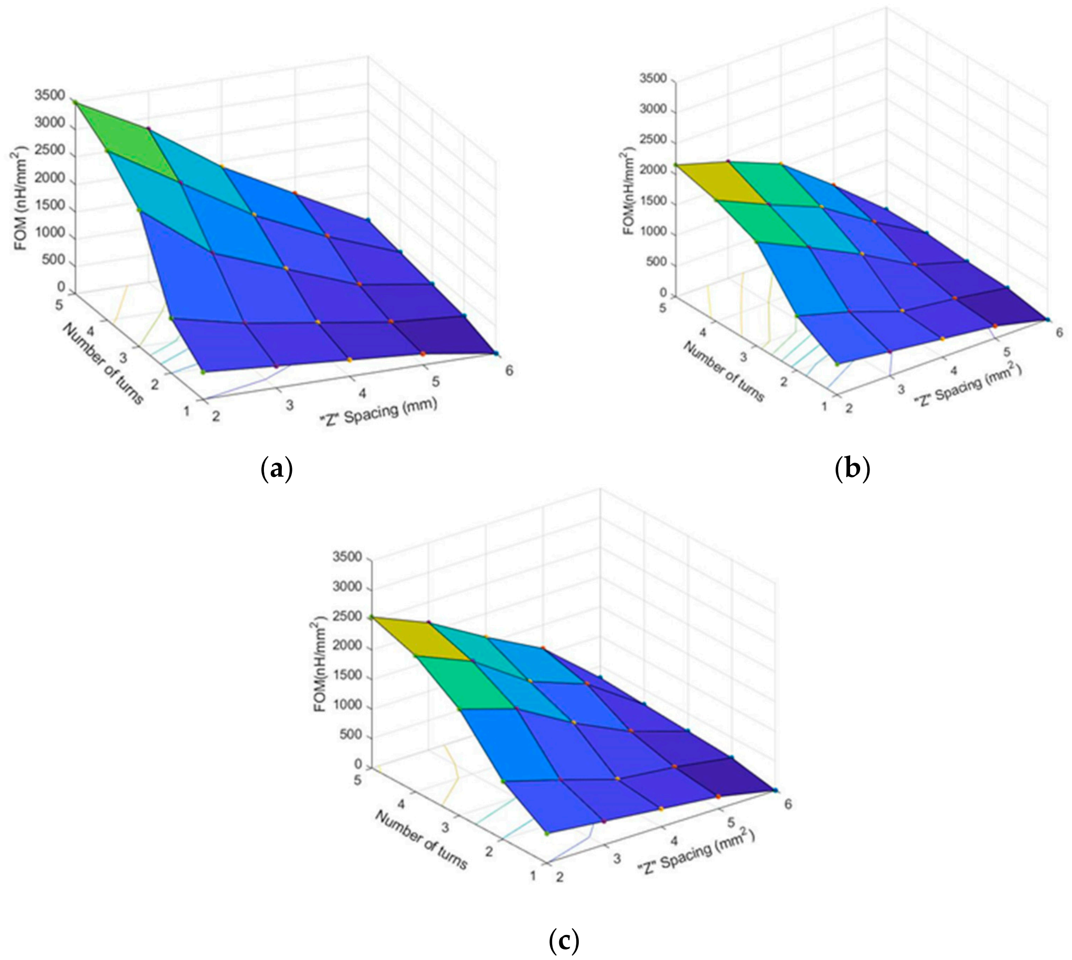

Figure 7. The Figure-Of-Merit (FOM) value as a function of number of turns and spacing between the coils for the square (**a**), hexagonal (**b**) and circular (**c**) designs, respectively.

3.3. The Uncertainty and Robust Design Results

The obtained results from the Ordinary and the Blind Kriging models for the optimum configuration (square) design (the best configuration) are shown in Figures 8 and 9, respectively. The 'Mean Squared Error' of the Leave-out cross validation was chosen to evaluate the quality of the fit as well as the predictive capability of the technique. These optimisation methods have both interpolated and extrapolated the data based on the short-term measurements from lab experiments. This is a very good way to predict the long-term behaviour based on short-term measurements. This saves time and cost associated with long experimental time and hence, it is favourable. In these plots, the response surface is constructed based on the equations of the Ordinary and Blind Kriging approaches whereas the dots are those simulated by the MATLAB code that randomly assigns the data points and runs the analysis through ANSYS, Figure 8a. As can be seen in Figure 8, the fit of the data is very good despite the small variances observed between the data points and the response surface, Figure 8b. However, an optimum region characterised by the highest inductance is observed when the distance between the coils, i.e., the Z spacing, is between 0.5 mm to 1.5 mm while the number of turns is between 37 and 60, Figure 8c. In this region, the highest inductance was above 20,000 μH.

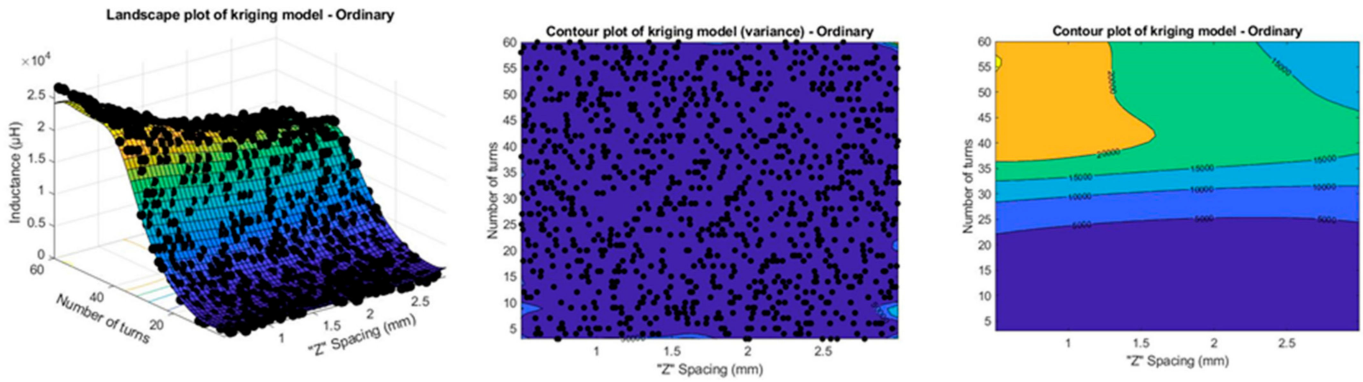

(**a**) (**b**) (**c**)

Figure 8. (**a**) The Ordinary Kriging response surface, (**b**) the variance plot and, (**c**) the contour plot of the inductance.

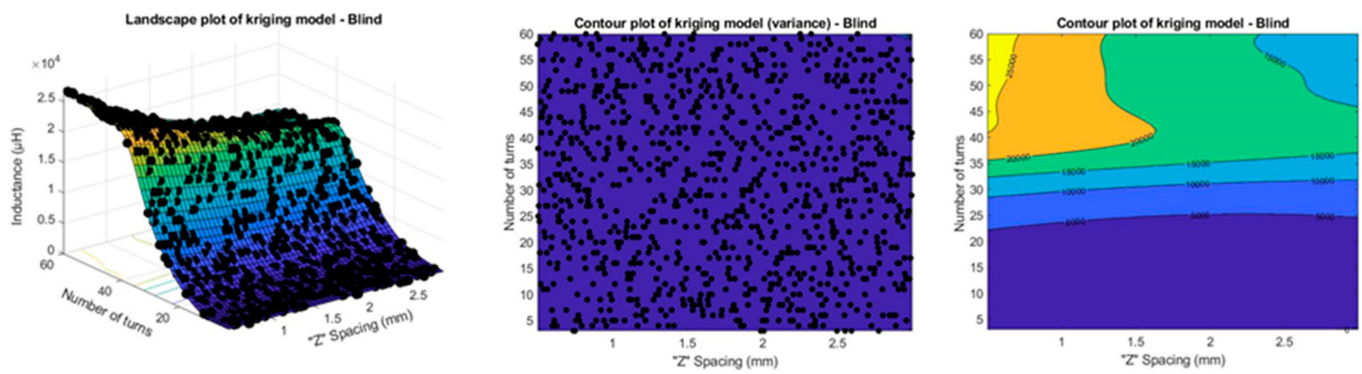

(**a**) (**b**) (**c**)

Figure 9. (**a**) The Blind Kriging response surface, (**b**) the variance plot and, (**c**) the contour plot of the inductance.

When looking the results of the blind kriging optimisation approach, it becomes evident that the fits, in general, are better with a lower level of variance compared to the ordinary kriging approach, Figure 9a,b. Moreover, it can be seen in Figure 9c that an optimum region of the highest inductance is observed (yellow-coloured zone) with values exceeding 25,000 μH. It is evident that the decrease in the spacing between the coils, i.e., the Z-spacing, as well as increasing the number of coils enhances the generated inductance.

4. Discussion of Results

The FEM displacement results in Figure 3 show the largest inductance value for the square coil, followed by the circular and hexagon coil. There are two distinct characteristics here, one for the square and circular coils and another for the hexagon coil. Lowest measurement range is for Hexagon coil, which is approximately of 0.5 mm, 1.5 mm and largest measurement range is for square and circular coils and is approximately equal to 0.2 mm. The hexagonal coil has the lowest measurement range with pitch of 1.5 mm. Contrary to this, the circular and square topologies having 1.5 mm pitch values, which is the lowest value. These are the lowest values of pitch for each topology, respectively.

The results of simulation show that alterations in topology of coil enable the sensitivity for matching the required range of displacement. The values of pitch chosen in this work significantly affect the inductance, but they do not have significant effect on shape of profile of signal-displacement. The decrease in value of pitch results in increase of number of turns and hence the induction as per expectation and this happens for circular and square coil topologies. There is a possibility that it is due to mutual inductance because interaction between tracks of copper increases due to area which becomes densely populated. It is obvious that changes in inductance are proportional to the self-inductance of planar coil so this value must be increased for optimizing displacement sensitivity.

Figure 4 shows the results of experiments which are obtained from measurements of actual displacement. Figure 5 shows that fabricated coils follow same trends for FEM counterparts. All the fabricated coils have greater values of inductance than that of simulated ones and circular and square coils topologies double the value of inductance. Square and circular coil topologies have irregularities in signal, and these are more obvious at greater pitch values but the correlation between these coils and the simulations are also good. Such type of irregularities is not visible in Hexagon topology. The data shown represent the inductance value of 80 kHz which lies in the range of 20 kHz to 100 kHz.

Signal to noise ratio is small for data which are below 20 kHz. In Figure 4, bars of errors have been removed. Impedance analyser is the main source of this error.

For further analysing performance of sensor, both experimental data and FEM were fitted with an exponential line with decaying trend. There is a more rapid decrease in inductance because the decay constant is larger for hexagon topology as compared to circular and square coils. Due to the non-linear nature of sensor, it is difficult to quantify sensitivity of the sensor. It can be seen that the spiral coil technologies have operating range which is greater in a displacement sensing application and have greater inductance value and sensitivity as well. Due to decrease in dimension of pitch, these parameters increase proportionally. These results show that for inductive sensing of displacement, planar coils use spiral coil topologies, ideally square, which has highest copper track density for sensor to perform better. However, design considerations are dependent on the application and it is difficult for general design rules to be applied as compared to the one mentioned above.

5. Conclusions

This paper presented a good correlation between the FE modelling simulation and the experimental measurements. A study of various shape of coils has been presented, using Ansys Maxwell simulation and experimentation. The topology of the coil has also an effect on the performance of the sensor. In total, three shapes of coils were designed, simulated and experimented to calculate the inductance and the magnetic flux density over various spacing distances. The different coil geometries generated different magnetic fluxes. The higher the magnetic flux the better the inductance. It has been observed that the inductance decreases with increasing the coils spacing distance. Comparing the performance of the three shapes, the square coil geometry has shown the best performance. Generally, the experimental measurements were very comparable with the analytical and FE modelling simulations. To optimise the design of the square geometry, optimisation models have been employed and the optimum values of the spacing distance and number of coils were obtained. That is, for the best configuration, i.e., the square design, the optimum spacing distance was between 0.5 mm to 1.5 mm while the optimum number of turns was between 37 and 60.

6. Patents

The novelty of the current paper stems from the fact that the proposed planar coil designs and sensor geometry have been modelled via Finite Element Modelling (FEM) alongside physical experimentation. This allows the model to be developed and validated for other designs in future to understand the performance and the influence of topologies when used in inductive sensing. The employed methodology has been applied to develop a novel displacement sensor. The models incorporated the development of an electromagnetic sensor via analysing the behaviour of the different planar coils that can be used as a part of a displacement sensor for tracking and location identification for the smart cities' applications. Furthermore, the models of different topologies with varying pitch values have been modelled using the ANSYS Maxwell. These models have been constructed and experimentally tested with various topologies, e.g., Hexagonal, Square and Circular. The correlation between the FEM models and the experimental data were significantly consistent which confirms that the methodology described here offers an effective way for developing a planar coil-based sensor with improved performance.

Author Contributions: Conceptualization and methodology, M.A. and B.Y.; software, validation and formal analysis, M.A.; writing—review and editing, M.A., B.Y. and D.Z. All authors have read and agreed to the published version of the manuscript.

Funding: This research received no external funding.

Acknowledgments: The author would like to thank Nada Aldoumani, Director of Innovative Technologies & Engineering Consultancy House (ITECH) Ltd., for her contribution towards the uncertainty quantification. Her efforts are highly appreciated and acknowledged.

Conflicts of Interest: The authors declare no conflict of interest.

References

1. Goldfine, N.J. Magnetometers for improved materials characterization in aerospace applications. *Mater. Eval.* **1993**, *51*, 396–405.
2. Anjomshoaa, A.; Duarte, F.; Rennings, D.; Matarazzo, T.J.; deSouza, P.; Ratti, C. City Scanner: Building and Scheduling a MobileSensing Platform for Smart City Services. *IEEE Internet Things J.* **2018**, *5*, 4567–4579. [CrossRef]
3. Bi, Y.; Govindaraju, M.R.; Jiles, D.C. The dependence of magnetic properties on fatigue in A533B nuclear pressure vessel steels. *IEEE Trans. Magn.* **1997**, *33*, 3928–3930. [CrossRef]
4. Shi, Y.; Jiles, D. Fem Analysis of the Influence of Fatigue Crack on Magnetic Properties of Steel. In Proceedings of the 1998 IEEE International Magnetics Conference (INTERMAG), San Francisco, CA, USA, 6–9 January 1998; p. 51.
5. Bi, Y.; Jiles, D.C. Dependence of Magnetic Properties on Crack Size in Steels. *IEEE Trans. Magn.* **1998**, *34*, 2021–2023. [CrossRef]
6. Varsier, N.; Plets, D.; Corre, Y.; Vermeeren, G.; Joseph, W.; Aerts, S.; Martens, L.; Wiart, J. A novel method to assess human population exposure induced by a wireless cellular network. *Bioelectromagnetics* **2015**, *36*, 451–463. [CrossRef] [PubMed]
7. Jow, U.; Ghovanloo, M. Design and Optimization of Printed Spiral Coils for Efficient Transcutaneous Inductive Power Transmission. *IEEE Trans. Biomed. Circuits Syst.* **2007**, *1*, 139–202. [CrossRef] [PubMed]
8. Siris, V.A.; Tragos, E.Z.; Petroulakis, N.E. Experiences with a metropolitan multiradio wireless mesh network: Design, performance, and application. *IEEE Commun. Mag.* **2012**, *50*, 128–136. [CrossRef]
9. Diez, L.; de Lope, L.R.; Agüero, R.; Corre, Y.; Stéphan, J.; Siradel, M.B.; Aerts, S.; Vermeeren, G.; Martens, L.; Joseph, W. Optimal Dosimeter Deployment into a Smart City IoT Platform for Wideband EMF Exposure Assessment. In Proceedings of the 2015 European Conference on Networks and Communications (EuCNC), Paris, France, 29 June–2 July 2015; pp. 528–532.
10. Hull, B.; Bychkovsky, V.; Zhang, Y.; Chen, K.; Goraczko, M.; Miu, A.; Shih, E.; Balakrishnan, H.; Madden, S. Cartel: A Distributed Mobile Sensor Computing System. In Proceedings of the 4th International Conference on Embedded Networked Sensor Systems, Boulder, CO, USA, 31 October–3 November 2006; pp. 125–138.
11. Van Le, D.; Tham, C.-K.; Zhu, Y. Quality of Information (QoI)—Aware Cooperative Sensing in Vehicular Sensor Networks. In Proceedings of the 2017 IEEE International Conference on Pervasive Computing and Communications Workshops (PerCom Workshops), Kona, HI, USA, 13–17 March 2017; pp. 369–374.
12. Primdahl, F. The fluxgate mechanism, part I: The gating curves of parallel and orthogonal fluxgates. *IEEE Trans. Magn.* **1970**, *6*, 376–383. [CrossRef]
13. Campolo, C.; Iera, A.; Molinaro, A.; Paratore, S.Y.; Ruggeri, G. SMaRTCaR: An Integrated Smartphone-Based Platform to Support Traffic Management Applications. In Proceedings of the 2012 First International Workshop on Vehicular Traffic Management for Smart Cities (VTM), Dublin, Ireland, 20–20 November 2012; pp. 1–6.
14. Mukhopadhyay, S.C.; Woolley, J.D.M.; Gupta, G.S. Inspecttiion off Saxophone Reeds Employing a Novell Planar Electromagnetic Sensing Technique. In Proceedings of the 2005 IEEE Instrumentation and Measurement Technology Conference Proceedings, Ottawa, ON, Canada, 16–19 May 2005; Volume 1, pp. 209–213.
15. Jolani, F.; Yu, Y.; Chen, Z. A Planar Magnetically Coupled Resonant Wireless Power Transfer System Using Printed Spiral Coils. *IEEE Antennas Wirel. Propag. Lett.* **2014**, *13*, 1648–1651. [CrossRef]
16. Mukhopadhyay, S.; Gooneratne, C. A Novel Planar-Type Biosensor for Noninvasive Meat Inspection. *IEEE Sens. J.* **2007**, *7*, 1340–1346. [CrossRef]
17. Mukhopadhyay, S.C.; Gooneratne, C.P.; Gupta, G.S.; Demidenko, S.N. A low-cost sensing system for quality monitoring of dairy products. *IEEE Trans. Instrum. Meas.* **2006**, *55*, 1331–1338. [CrossRef]
18. Mukhopadhyay, S.; Yamada, S.; Iwahara, M. Inspection of electroplated materials–performance comparison with planar meander and mesh type magnetic sensor. *Int. J. Appl. Electromagn. Mech.* **2002**, *15*, 323–329. [CrossRef]
19. Mukhopadhyay, S.C. Quality inspection of electroplated materials using planar type micro-magnetic sensors with post-processing from neural network model. *IEE Proc.-Sci. Meas. Technol.* **2002**, *149*, 165–171. [CrossRef]
20. Gooneratne, C.; Mukhopadhyay, S.C.; Purchas, R.; Gupta, G.S. Interaction of Planar Electromagnetic Sensors with Pork Belly Cuts. In Proceedings of the 1st International Conference on Sensing Technology, Palmerston North, New Zealand, 21–23 November 2005.
21. Mukhopadhyay, S.C. A novel planar mesh type micro-electromagnetic sensor: Part II–estimation of system properties. *IEEE Sens. J.* **2004**, *4*, 308–312. [CrossRef]
22. Mamishev, A.; Sundara-Rajan, K.; Yang, F.; Du, Y.; Zahn, M. Interdigital sensors and transducers. *Proc. IEEE* **2004**, *92*, 808–845. [CrossRef]

23. Fratticcioli, E.; Dionigi, M.; Sorrentino, R. A Planar Resonant Sensor for the Complex Permittivity Characterization of Materials. In Proceedings of the 2002 IEEE MTT-S International Microwave Symposium Digest, (Cat. No.02CH37278). Seattle, WA, USA, 2–7 June 2002; pp. 647–649.
24. Toda, K.; Komatsu, Y.; Oguni, S.; Hashiguchi, S.; Sanemesa, I. Planar gas sensor combined with interdigitated array electrodes. *Anal. Sci.* **1999**, *15*, 87–89. [CrossRef]
25. Timmer, B.H.; Sparreboom, W.; Olthuis, W.; Bergveld, P.; van den Berg, A. Planar interdigitated conductivity sensors for low electrolyte concentrations. In *Proceedings Semiconductor Sensor and Actuator Technology, SeSens, Veldhoven*; STW: Utrecht, The Netherlands, 2001; pp. 878–883.
26. Yoon, S.; Sim, J.K.; Cho, Y.H. On-Chip Flexible Multi-Layer Sensors for Human Stress Monitoring. In Proceedings of the IEEE SENSORS 2014, Valencia, Spain, 2–5 November 2014; pp. 851–854.
27. Gramacy, R.B.; Lee, H.K.H. Gaussian Processes and Limiting Linear Models. *Comput. Stat. Data Anal.* **2008**, *53*, 123–136. [CrossRef]
28. Paciorek, C.J. Nonstationary Gaussian Processes for Regression and Spatial Modelling. Ph.D. Thesis, Carnegie Mellon University, Pittsburgh, PA, USA, 2003.
29. Sakata, A.; Ashida, F.; Zako, M. Structural optimization using kriging approximation. *Comput. Meth. Appl. Mech. Eng.* **2003**, *192*, 923–939. [CrossRef]
30. Chady, T.; Enokizono, M.; Sikora, R. Neural network models of eddy current multi-frequency systems for nondestructive testing. *IEEE Trans. Magn.* **2000**, *36*, 1724–1727.
31. Chady, T.; Enokizono, M.; Sikora, R.; Todaka, T.; Tsuchida, Y. Natural crack recognition using inverse neural model and multi-frequency eddy current method. *IEEE Trans. Magn.* **2001**, *37*, 2797–2799. [CrossRef]
32. Alexander, F.; András, S.; Andy, K. *Engineering Design Via Surrogate Modelling*; University Southampton: Southampton, UK, 2008; ISBN 9780470770795.
33. Joseph, V.R.; Hung, Y.; Sudjianto, A. Blind kriging: A new method for developing metamodels. *ASME J. Mech. Des.* **2008**, *130*, 031102:1–031102:8. [CrossRef]
34. Razavi, S.; Tolson, B.A.; Burn, D.H. Review of surrogate modeling in water resources. *Water Resour. Res.* **2012**, *48*, W07401. [CrossRef]
35. Jack, P.C.K. *Kriging: Methods and Applications*; Tilburg University: Tilburg, The Netherlands, 2017.